A High Power Density Thermal Management Approach Using Multi-PCB Distributed Cooling (MPDC) Structure

Wenbo Liu, Andrew Yurek, Yang Chen, Bo Sheng, Xiang Zhou and Yan-Fei Liu, *Fellow, IEEE*
Department of Electrical and Computer Engineering
Queen's University, Kingston, Canada
liu.wenbo@queensu.ca, yanfei.liu@queensu.ca

Abstract — This paper presents a new thermomechanical PCB design that uses a multi-PCB cooling (MPDC) structure to achieve higher power density while maintaining thermal performance. The new MPDC structure focusses on three design principles: multiple vertically stacked PCB's for more efficient use of space, component sorting based on losses for improved cooling, and integrated liquid cooling for maximum thermal dissipation. Liquid cooling method is utilized to implement the thermal management problem with very high power density. Finite element analysis (FEA) based thermal analysis was conducted on the 1.3kW converter with two-PCB integrated liquid cooling model. Same thermal estimation as single PCB structure was verified. An experimental prototype with one PCB and cooling setup with liquid and air cooling was built. A 1.3 kW LLC power converter was developed, 50% less temperature rise on critical devices and 0.6% better efficiency are achieved. Thereafter, the proposed MPDC structure was investigated based the single PCB design. The two-layer MPDC prototype repeats the same efficiency and thermal performance while achieving 31% improvement in power density.

Keywords – high power density, liquid cooling, multi-layer structure

I. INTRODUCTION

Advanced power converters with high power density are demanded in a wide range of power levels, especially in the field of portable devices, computer point of load supplies, unmanned drones and electrified transportation systems [1][2]. Therefore, research has focussed on improving the power density and miniaturizing the total converter size for different applications. Integration technologies are studied to combine the passive devices and active components, to build more compact structures [3][4]. Designs are implemented with wide band gap (WBG) devices and high frequency magnetics which reduce the size of bulky passive components by allowing for higher operating switching frequency [5][6][7]. With the development of device technologies and the improvement of the fabrication process, the power density of various types of power electronic supplies is growing continuously.

Size reduction has come at the cost of increased power consumption. Consequently, the primary limitation in meeting this demand of power density is thermal management [8]. As the overall size of the passive and electronic components decrease, losses in these components increase and surface area available to dissipate heat decreases. The combination of increased loss and decreased surface area poses a difficult challenge for the thermal design of the converters. To fulfill the potential of emerging high-density technologies, thermal management solutions for integrated device and power modules are strongly desired. Various cooling methods are proposed which target conduction or convection heat transfer improvements based on appropriate cases. High thermal conductivity materials are utilized to reduce the temperature rise of fully integrated modules. High current IGBT power modules use modified double sided cooling and a thick copper bonding structure to increase the surface area for better convection performance [9][10]. Studies on enhanced air cooling with high liquid flow meter (LFM) are investigated to enable more efficient and adaptive air flow design.

For medium power level converters ranging from 1kW to 20kW, such as electric vehicle applications which require both high power and compact size, a single solution of conduction or convection cooling is insufficient [11][12]. Liquid cooling solutions combine both conduction and convection features and is therefore widely used in power supply applications. Decreased temperature rise is accomplished with the low thermal resistance of a liquid cooling system to transfer more heat generated by relatively high power [13]. Numerous researches have focussed on improving existing liquid cooling methods regarding the considerations of cost, size and reliability. A proposed design integrates both the functions of heatsink and pump to achieve smaller volume [14]. In [15] and [16], different copper cold plate heatsink technologies are compared based on thermal performance. In [17], thermal expansion is addressed to maintain the long-term lifespan of the liquid cooling loop. Research has also focused on different coolants to improve heatsinking [18].

Although liquid cooling technology is well developed for integrated circuits (ICs) and high-power semiconductor modules, few solutions are available for power converters on print circuit board (PCB) assemblies. These medium-power level converters are composed of PCB, semiconductor devices, passive components and control circuitry. Thus,

they have complicated 3D layouts. Industrial and academic research has either focused on improving the discrete component cooling or PCB design exclusively instead of redesigning both aspects together. Furthermore, these conventional methods consume excessive space, therefore power density must be decreased to accommodate the liquid cooling unit.

To achieve optimal thermal performance while minimizing device volume, a new multi-PCB cooling (MPDC) structure is proposed. A two-PCB structure is designed to make more efficient use of space based on separating power semiconductor devices, magnetics and low loss control circuit. This paper is organized into the following sections: Section II describes the MPLC structure principle, which is applied to a studied power converter; Section III presents finite element analysis (FEA) thermal results for liquid cooling performance proof; Section IV presents the lab protype with experimental results, as well as the two-PCB simulation verification and experimental verification. Section V concludes the paper.

II. PRINCIPLE OF MPDC STRUCTURE

The proposed MPDC technology is demonstrated on a 1.3kW LLC power converter. This converter is designed for high voltage to low voltage conversion and the rated power is 14V output at 95A maximum load current. The specifications are shown in TABLE I. In order to decrease the high output current stress, a two-transformer structure shown in Fig. 1 is used to distribute the loading [19]. Benefiting from the high frequency features of GaN devices, this converter can operate in high frequency to achieve high power density and high efficiency[20][21]. Liquid cooling solution is implemented on this layout with the cold plate bonded to the bottom side of PCB, and the entire bottom surface has been left blank for the installation. Conventional one-PCB structure layout must accommodate both footprints of passive component and active switches on the top layer of PCB as shown in Fig. 2. It can be observed from the top view of layout that either the magnetics or the switches takes half of the area. Also, an external daughter card is required to implement the placement of control circuit due to the limited area of mother board.

The objective of MPDC is to use package volume more efficiently to reduce volume while maintaining thermal performance by still leaving the bottom surface blank. This structure focusses on three design principles to achieve these objectives. First, MPDC uses two or more PCB's connected vertically through copper connections to make use of three-
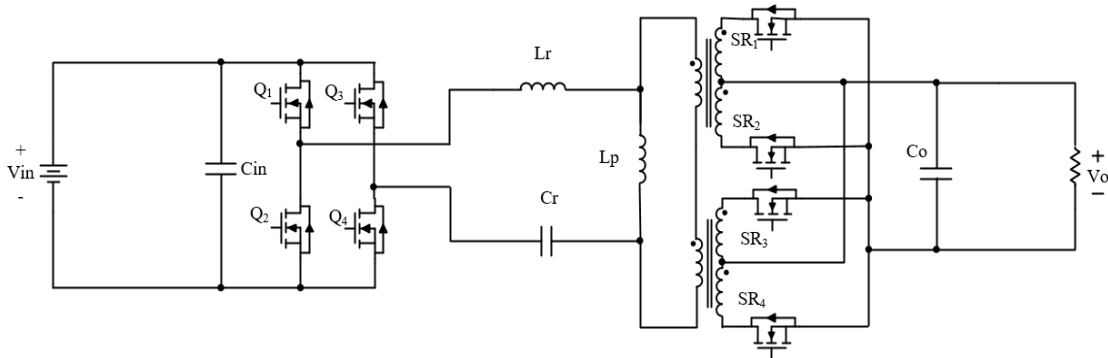

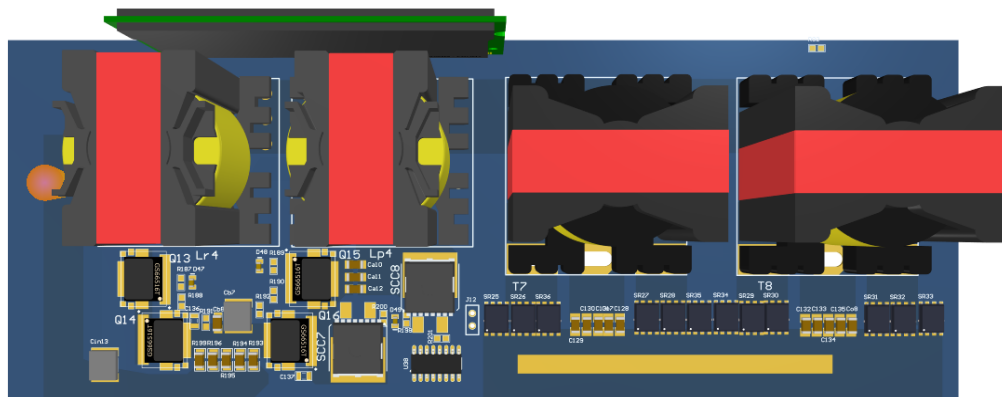Fig. 1. Target LLC converter topology with two transformers

Fig. 2. Top view of conventional single PCB converter layout

TABLE I. PARAMETERS OF THE STUDIED LLC CONVERTER

V_{in}	Output voltage V_{out}	Maximum current I_{out}	Switching frequency f_{sw}	Dissipated heat P_d	Dimensions one PCB (mm)	Dimensions two PCBs (mm)
400V	14V	95A	260~350kHz	55W	70*190*42	45*190*50

dimensional space and create more surface area to accommodate footprints of components. Second, MPDC sorts components by heat generation and distributes components according to these properties, and the high loss components are bonded to copper heat spreaders to dissipate the heat downwards. Finally, MPDC incorporates liquid cooling through a cold plate heatsink attached to the bottom side of the bottommost PCB.

Fig. 3 shows the complete MPDC structure in block diagrams. MPDC allows for efficient placement of components according to loss. The top board is reserved for large magnetic components and low loss circuitry that provides control functions. Magnetic components are connected to the bottom board using copper connections electrically connected to both PCB layers. These connections also serve to anchor the bulky magnetic components to both PCB layers for support. On the bottom PCB layer, high loss surface mount components are exclusively placed on the top side to provide direct connection to the cold plate heatsink. Component height should be minimized to reduce the gap
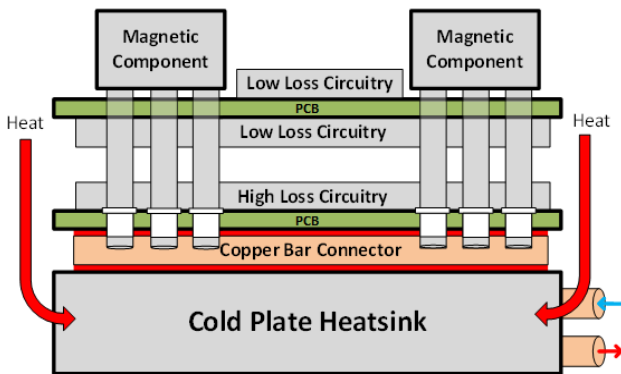
between PCBs and therefore minimize package volume. The entire bottom side of the bottom PCB is used to connect to the heatsink, except in areas with vertical copper connector protrusions.

Finally, MPDC incorporates active liquid cooling via a cold plate heatsink attached to the bottom side of the bottom PCB to transfer heat away from the converter. This connection is composed of the liquid cooled cold plate heatsink, thermal gap pads, copper bar connectors, and the bottom PCB. Copper bars allow a flush connection between the cold plate and PCB. Thermal gap pads are used to provide uniform contact, electric isolation and compensation of CTE mismatch. Two-layer structure allows for the width of the converter to be significantly reduced while increasing the overall height by a small amount. Therefore, package volume is significantly decreased. In the conventional one-PCB structure, the total size is 0.56L with power density of 2.33kW/L; while for the MPDC converter it achieves 0.43L and 3.15kW/L power density. 31% of size is reduced benefiting from the design of component placement with same performance and liquid cooling solution.

Fig. 4 and Fig. 5 show the top views of the two PCBs in MPDC structure, magnetics locate on the top side of top PCB and the switches are on the top side of bottom PCB. Fig. 6 shows the front cross section view of two-PCB stack. More space can be used, and control circuit locates on the bottom side of the top PCB. A liquid cooling cold plate is assembled underneath the MPDC configured prototype with copper bar connection. The component size, surface area and contact area with the liquid cooling system in MPDC structure are the same as that in a one-PCB structure, thus the same thermal performance can be achieved.

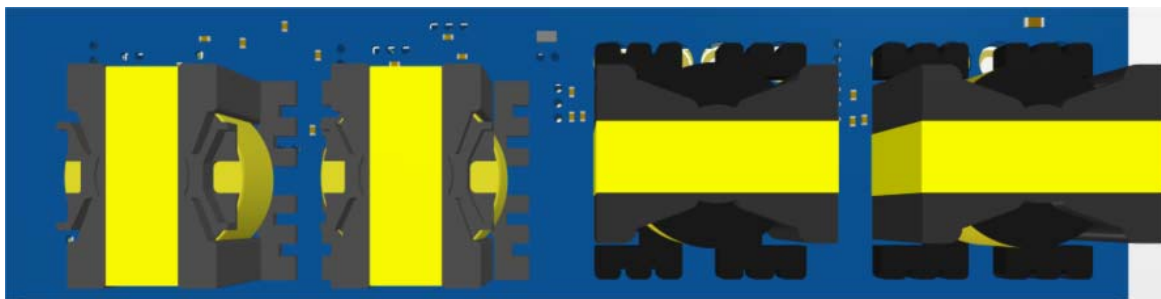Fig. 3. Block diagram of MPDC structure

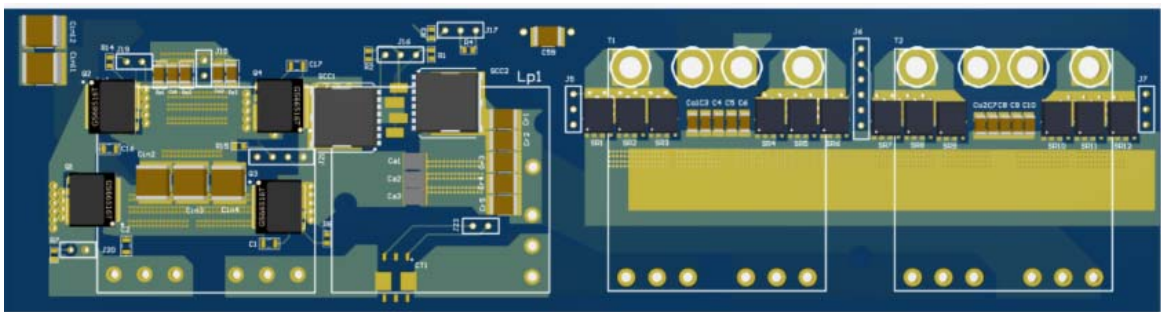Fig. 4. Top view of MPDC top PCB with magnetic components

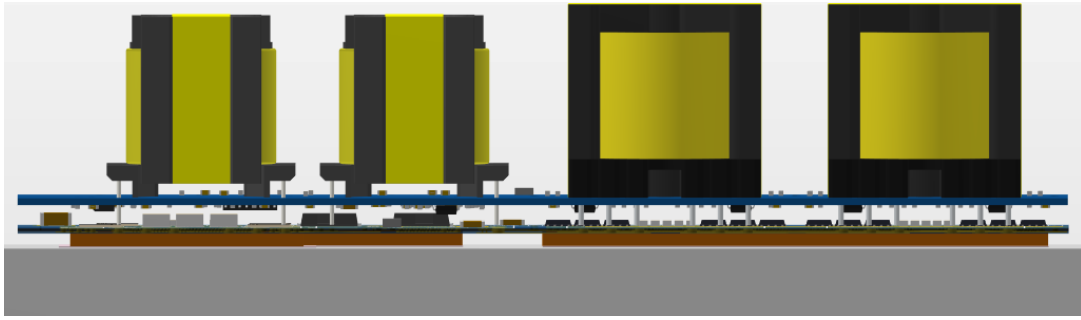Fig. 5.   Top view of MPDC bottom PCB with semiconductor devices.

Fig. 6. Front view of MPDC converter with liquid cooling assembly.

III. Modeling and FEA Thermal Estimation Comparison

A. Loss breakdown

To verify the thermal performance of MPDC liquid cooling system, FEA simulation is used by estimating the operating temperature. Three sets of simulation are performed: #1 conventional single PCB air cooled converter, #2 single PCB liquid cooled converter, and #3 MPDC liquid cooled converter. Three-dimensional models for each condition are created while the loss breakdown of the converter is also analyzed.

The operating condition for all three simulation cases is 380V input, 14V output with 95A load current. The loss of LLC converter is estimated and divided amongst 6 major components: primary side switches loss (conduction loss and switching loss of GaN FETs), resonant inductor (L_r) winding loss and core loss; parallel inductor (L_p) winding loss and core loss; transformer loss (including primary and secondary winding loss, core loss of two transformers); secondary side synchronous rectifier (SR) switches loss and secondary side PCB copper loss.

The losses are estimated based on the existing literatures. The current and voltage values of each of the power components are simulated with PSIM software, while the static and dynamic properties are extracted from the datasheets. The conduction loss and switching loss of GaN FETs are calculated based on I^2R and gate charging information. C_{oss} loss is estimated based on the discussion in [22]. For the magnetic components, their core losses are calculated by Steinmetz's equation; the AC copper loss in high frequency is analyzed based on the study of proximity effect and skin effect in [23][24]. Transformer secondary side winding loss is estimated based on [25]. SR conduction loss is calculated with RMS current and turn-on resistance of MOSFETs. The turn-on time is assumed to be 75% of the whole switching period considering the delay of SR current sensing circuit. No switching loss is considered because the LLC converter operates in the secondary side zero current crossing mode. The losses on the PCB copper and equivalent series resistor (ESR) of output filter capacitors are estimated based on the previous experience.

With the losses are estimated, the loss breakdown and values are shown in TABLE II. The loss distribution in the MPDC model is the same as the single layer converter. The losses are assigned in the same components.

TABLE II. Loss Breakdown of Stuided LLC Converter

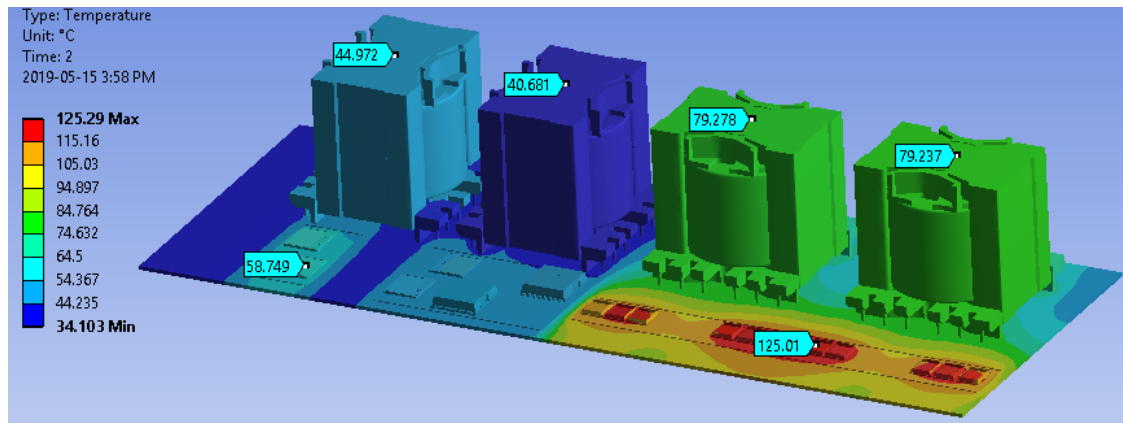| Dissipated heat P_d	GaN FET loss P_{GaN}	Resonant L loss P_{Lr}	Parallel L loss P_{Lp}	Transformer loss P_{Tx}	Secondary SR loss P_{SR}	Secondary PCB loss P_{SP}	Capacitor ESR loss P_C
51.86W	3.49W	3.34W	2.61W	16.38W	19.51W	4.53W	2W

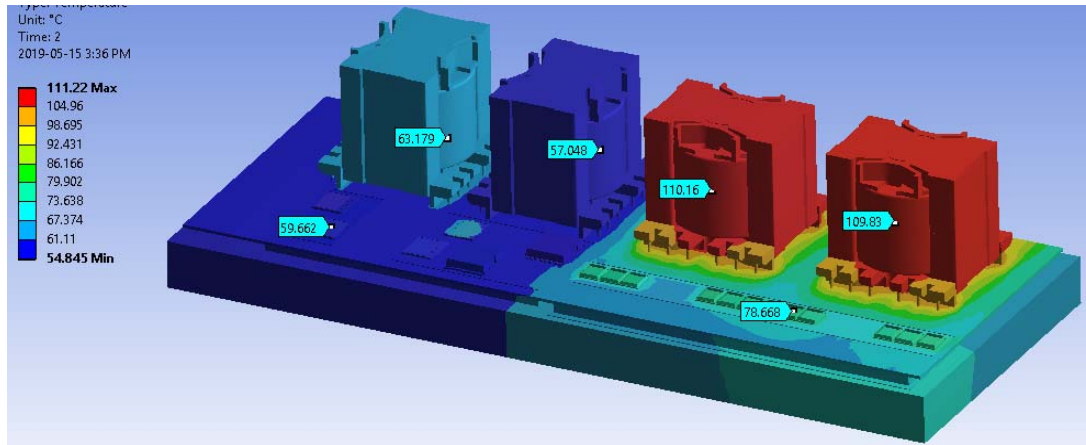Fig. 6. Thermal simulation of single PCB air cooled layout.

4184

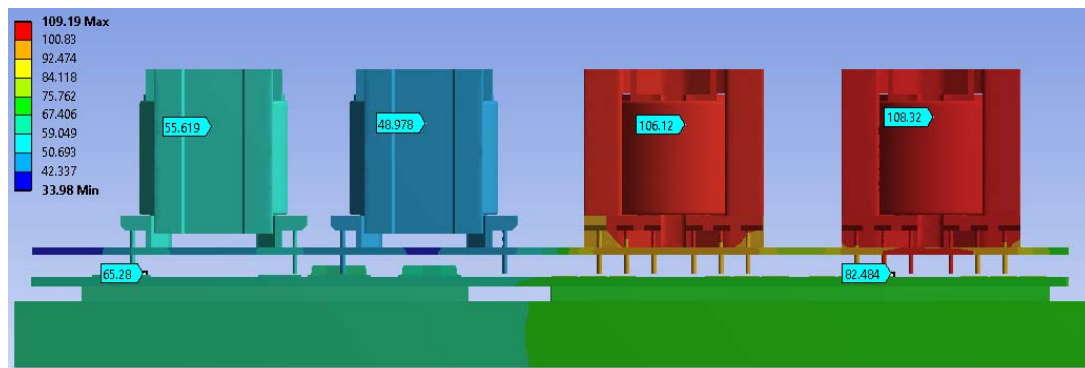Fig. 7. Thermal simulation of single PCB liquid cooled layout

Fig. 8. Thermal simulation of MPDC liquid cooled layout.

B. FEA thermal simulation results

The results of Fig. 6 to Fig. 8**Error! Reference source not found.** show the temperatures of the transformers (T_x), series inductor (L_r), parallel inductor (L_p), primary side rectifier GaN switches (GaN), and synchronous rectifiers (SR) of the power converter. All three cases are simulated under 25°C ambient temperature. Fig. 6 represents the simulated temperatures with air cooling. The heat coefficient of moving air convection is assumed to be four times higher than still air. It can be observed from the figure that the maximum temperature of secondary SR MOSFETs is 125°C, which is very close to the device tolerance. The magnetic components are well cooled under 80°C due to the air cooling of the bulky cores with large surface area.

Fig. 7 shows the estimation based on the conventional single PCB liquid cooling assembly. The maximum temperature on the semiconductor switches and PCB is 79°C, indicating a reduction of temperature rise by 50% (54°C with liquid cooling versus 100°C with air cooling). The temperature of magnetic components is higher because the design target of this liquid cooling system is focusing on the surface mount switches. However, the passive components are much less sensitive compared to the semiconductor devices, thus the reliability and efficiency are expected to be improved. This claim will be investigated by experiments in the following section.

Fig. 8 shows the thermal performance of MPDC converter layout with the same losses and ambient temperature. Compared with Fig. 7, the MPDC structure achieves almost the same thermal performance on the GaN FETs, the SR MOSFETs and the magnetic components. The temperature of active switches is significantly decreased compared with the air-cooling solution while the size is 30% smaller than the single PCB converter.
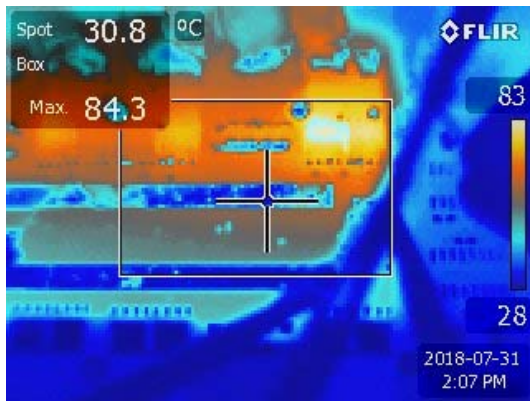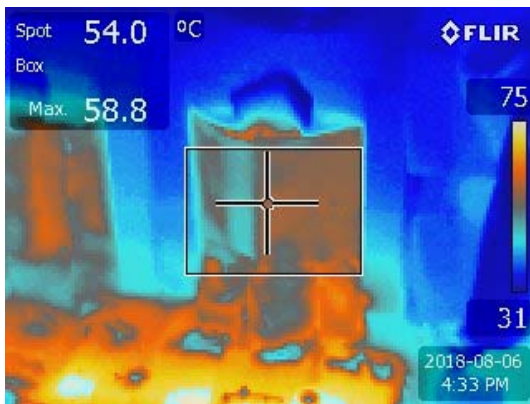
IV. VERIFICATION WITH EXPERIMENTAL RESULTS

A prototype of the two-layer MPDC power converter is manufactured to perform the experimental verification on performance and temperature. Another prototype with all the same components but a single PCB is also built. Thermal testing has been conducted on #1 single-layer PCB with air cooling #2 single layer PCB using liquid cooling and #3 two-layer MPDC power converter with liquid cooling. The liquid cooling loop consists of a pump, reservoir, radiator with fans and a cold plate, water is used as the coolant in the experiment. The prototypes are implemented with a 1.3kW

(a) Temperature of SR MOSFETs.

(b) Temperature of transformers

Fig. 9. Temperature at 70A load current with air cooling

Fig. 10. SR temperature at 95A load current with air cooling

power converter as discussed in TABLE I. Testing #1 operates at 14V output / 70A load current steady-state condition and 95A for a short-period verification. Testing #2 and #3 are tested with 95A full load stead state condition.

Fig. 9 illustrates the 70A steady state air cooling thermal performances in the thermal images of testing #1. The maximum temperature of the passive components is 59°C on the transformer secondary winding; and the maximum temperature of semiconductor devices is 84°C on the SR MOSFETs. Once the load current is increased to 95A for one-minute short period, the temperature of SR MOSFETs rises to 122°C very quickly as shown in Fig. 10. Therefore, the safe loading capability with air cooling solution is around 70A and the full load condition has already exceeded the limitation of heat dissipation.

(a)Temperature of SR MOSFETs

(b)Temperature of GaN.
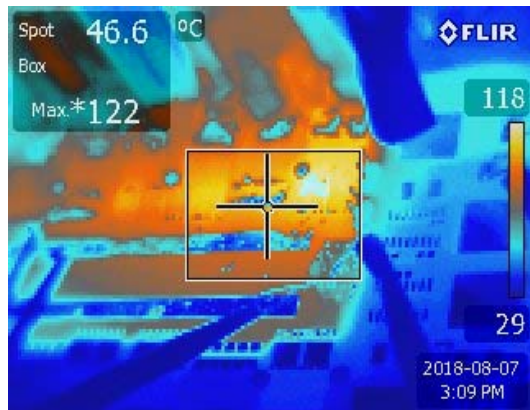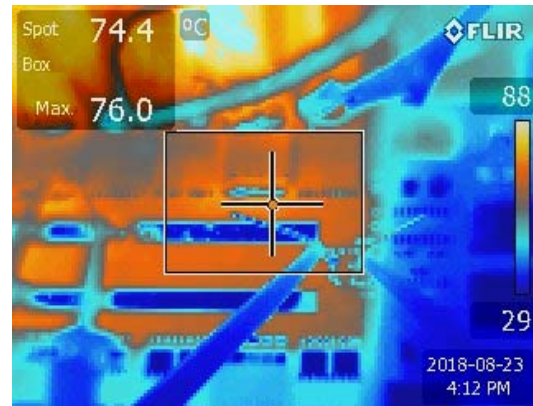Fig. 11. Temperature at 95A load current with liquid cooling

Fig. 11 and Fig. 12 demonstrate the significantly improved thermal performance achieved by single-PCB liquid cooled converter and MPDC converter respectively. Thus, the maximum steady state operating temperature of active devices with liquid cooling is 76°C on the SR MOSFETs, which is more than 46°C lower than air cooled SRs at 95A load current. The temperature of transformer is 110°C, but the passive devices are less sensitive as they have higher temperature ratings. Thermal image of switches in the MPDC prototype is not applicable but the temperature of magnetic components matches with the single PCB results
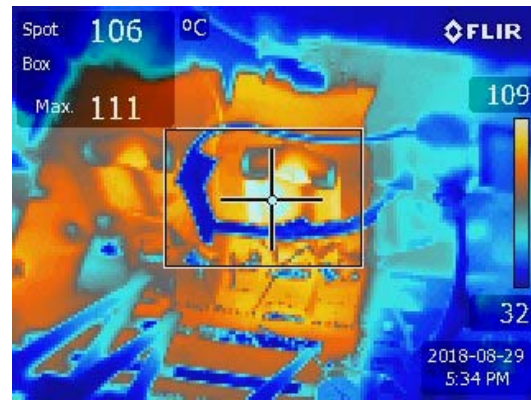
very closely. Therefore, SR and GaN temperatures are expected to remain unchanged.

Benefiting from the lower temperature rise, the on-state resistance of SR MOSFETs is reduced and therefore the power loss generated by the high load current can be reduced. The efficiency curves of air-cooled and liquid-cooled prototypes are shown in Fig. 13. It can be concluded from the testing results that the efficiency at 70A load current condition is improved by 0.6% (96.1% compared with 95.5%). As 95A full load is an abnormal overload condition for air-cooled prototype, the efficiency is not comparable at full load. But even bigger difference can be expected as the loading is getting heavier.

Basically, the experimental results of air-cooled and liquid-cooled converter show a close agreement with the FEA simulation. The liquid cooling solution achieves 48% temperature rise reduction on the hot spot of active devices, increases the loading capability and improves the efficiency by 0.6%. Also, the 1.3kW power converter with MPDC improves the total package power density by 31% compared to the single PCB layer design.

V. CONCLUSION

This paper proposes a new multi-PCB distributed cooling (MPDC) structure for discrete power converters based on multiple PCB layers and liquid cooled solution. MPDC improves package volume without sacrificing thermal performance based on three design principles: multiple vertically stacked PCB's to use three-dimensional space more efficiently, component sorting by loss to cool down the critical parts and increase the size of heat spreader through a bottom mounted cold plate for thermal dissipation. FEA thermal modelling is conducted on a 1.3kW power converter. Experimental results of air cooling and liquid cooling are compared to verify the heatsinking abilities of the MPDC structure. Integrated liquid-cooling reduces synchronous rectifier (SR) temperatures by 46°C in experimental results and improves the efficiency by more than 0.6%. A power converter with two-layer MPDC has been designed and achieves 31% greater power density than the single-layer design.

(a) Temperature of transformers.

(b)Temperature of Inductors.
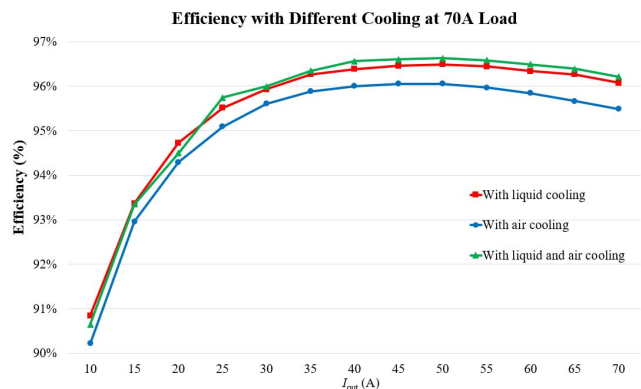
Fig. 12. Temperature at 95A load current with MPDC

Fig. 13. Comparison of efficency with different cooling solution

REFERENCES

[1] F. C. Lee and Q. Li, "High-Frequency Integrated Point-of-Load Converters: Overview," in *IEEE Transactions on Power Electronics*, vol. 28, no. 9, pp. 4127-4136, Sept. 2013.

[2] C. Duan, H. Bai, W. Guo and Z. Nie, "Design of a 2.5-kW 400/12-V High-Efficiency DC/DC Converter Using a Novel Synchronous Rectification Control for Electric Vehicles," in *IEEE Transactions on Transportation Electrification*, vol. 1, no. 1, pp. 106-114, June 2015

[3] Z. Liu, B. Li, F. C. Lee and Q. Li, "High-Efficiency High-Density Critical Mode Rectifier/Inverter for WBG-Device-Based On-Board Charger," in *IEEE Transactions on Industrial Electronics*, vol. 64, no. 11, pp. 9114-9123, Nov. 2017.

[4] L. Wang, W. Liu, D. Malcom and Y. Liu, "An Integrated Power Module Based on the Power-System-In-Inductor Structure," in *IEEE Transactions on Power Electronics*, vol. 33, no. 9, pp. 7904-7915, Sept. 2018.

[5] W. Zhang, F. Wang, D. J. Costinett, L. M. Tolbert and B. J. Blalock, "Investigation of Gallium Nitride Devices in High-Frequency LLC Resonant Converters," in *IEEE Transactions on Power Electronics*, vol. 32, no. 1, pp. 571-583, Jan. 2017

[6] J. L. Lu, D. Chen and L. Yushyna, "A high power-density and high efficiency insulated metal substrate based GaN HEMT power module," 2017 *IEEE Energy Conversion Congress and Exposition (ECCE)*, Cincinnati, OH, 2017, pp. 3654-3658.

[7] J. L. Lu, R. Hou and D. Chen, "Opportunities and design considerations of GaN HEMTs in ZVS applications," 2018 *IEEE Applied Power Electronics Conference and Exposition (APEC)*, San Antonio, TX, 2018, pp. 880-885

[8] L. Boteler, "Thermal Design of Power Electronics," *2019 IEEE Applied Power Electronics Conference and Exposition (APEC)*, Anaheim, CA, 2019, Educational Tutorial.

[9] Z. Liang, P. Ning, F. Wang and L. Marlino, "A Phase-Leg Power Module Packaged with Optimized Planar Interconnections and Integrated Double-Sided Cooling," in *IEEE Journal of Emerging and Selected Topics in Power Electronics*, vol. 2, no. 3, pp. 443-450, Sept. 2014.

[10] Numakura, K., Emori, K., Yoshino, Y., Hayami, Y., Hayashi, T., (2016, September). Direct-cooled power module with a thick Cu heat spreader featuring a stress-suppressed structure for EV/HEV inverters. In 2016 *IEEE Energy Conversion Congress and Exposition (ECCE)*. IEEE.

[11] R. Hou and A. Emadi, "Applied Integrated Active Filter Auxiliary Power Module for Electrified Vehicles with Single-Phase Onboard Chargers," in *IEEE Transactions on Power Electronics*, vol. 32, no. 3, pp. 1860-1871, March 2017

[12] R. Hou and A. Emadi, "A Primary Full-Integrated Active Filter Auxiliary Power Module in Electrified Vehicles with Single-Phase Onboard Chargers," in *IEEE Transactions on Power Electronics*, vol. 32, no. 11, pp. 8393-8405, Nov. 2017

[13] M. Vuckovic and N. Depret, "Impacts of local cooling technologies on air cooled data center server performance: Test data analysis of Heatsink, Direct Liquid Cooling and passive 2-Phase Enhanced Air Cooling based on Loop Heat Pipe," 2016 32nd *Thermal Measurement, Modeling & Management Symposium (SEMI-THERM)*, San Jose, CA, 2016, pp. 71-80.

[14] F. Liu, B. Duan, X. Yu, R. Wu and X. Luo, "A study on a simplified liquid cooling system with a pump serving as cold plate," in *International Conference on Electronic Packaging Technology (ICEPT)*, Harbin, China, 2017.

[15] B. Akselband, K. Whitenack and D. Goldman, "Copper Cold Plate Technology Comparison," in *Thermal and Thermomechanical Proceedings 10th Intersociety Conference on Phenomena in Electronics Systems*, San Diego, CA, 2006.

[16] K. Hwang, S. W. Lee, S. W. Karng and S. Y. Kim, "Thermal performance of non-metallic two-phase cold plates for humanoid robot cooling," in *Intersociety Conference on Thermal and Thermomechanical Phenomena in Electronic Systems*, Orlando, FL, 2008.

[17] M. Parlak and V. Yagci, "Thermal Expansion Investigation of Liquid Cold Plate with Varying Ambient Temperature at Storage," in *IEEE Intersociety Conference on Thermal and Thermomechanical Phenomena in Electronic Systems (ITherm)*, San Diego, CA, 2018.

[18] G. R. Wagner, J. R. Schaadt, J. Dixon, G. Chan, W. Maltz, K. Mostafavi and D. Copeland, "Test results from the comparison of three liquid cooling methods for high-power processors," in *IEEE ITHERM Conference*, Las Vegas, 2016.

[19] Z. Hu, Y. Qiu, L. Wang and Y. Liu, "An Interleaved LLC Resonant Converter Operating at Constant Switching Frequency," *in IEEE Transactions on Power Electronics*, vol. 29, no. 6, pp. 2931-2943, June 2014.

[20] Y. Kim, C. Oh, W. Sung and B. K. Lee, "Topology and Control Scheme of OBC–LDC Integrated Power Unit for Electric Vehicles," in *IEEE Transactions on Power Electronics*, vol. 32, no. 3, pp. 1731-1743, March 2017

[21] Z. Liu, R. Yu, T. Chen, Q. Huang and A. Q. Huang, "Real-time adaptive timing control of synchronous rectifiers in high frequency GaN LLC converter," *2018 IEEE Applied Power Electronics Conference and Exposition (APEC)*, San Antonio, TX, 2018, pp. 2214-2220.

[22] G. Zulauf, S. Park, W. Liang, K. N. Surakitbovorn and J. Rivas-Davila, "COSS Losses in 600 V GaN Power Semiconductors in Soft-Switched, High- and Very-High-Frequency Power Converters," in *IEEE Transactions on Power Electronics*, vol. 33, no. 12, pp. 10748-10763, Dec. 2018.

[23] C. R. Sullivan and R. Y. Zhang, "Simplified design method for litz wire," *2014 IEEE Applied Power Electronics Conference and Exposition - APEC 2014*, Fort Worth, TX, 2014, pp. 2667-2674.

[24] W. Liu, L. Wang, S. Webb, Y. F. Liu and D. Malcolm, "A Modified Equivalent Circuit Based Electro-Thermal Model for Integrated POL Power Modules," in *IEEE Energy Conversion Congress & Expo (ECCE) 2017*, Cincinati,Ohio, USA, Oct 2017, pp. 1366-1373

[25] Hu Wenshan, Yi Lingsong, Liu Zhiwei and Yan Hui, "Loss analysis and improvement of all parts of magnetic resonant wireless power transfer system," 2015 Chinese Automation Congress (CAC), Wuhan, 2015, pp. 2251-2256.